

Article

Closure of the Eastern Paleo-Asian Ocean: Constraints from the Age and Geochemistry of Early Permian Zhaojinggou Pluton in Inner Mongolia (North China)

Guang-Yao Li ^{1,2,3}, Liang Qiu ^{3,*} , Zhi-Dan Li ^{1,2,*}, Lei Gao ³, Chao Fu ^{1,2}, Jia-Ying Wang ^{1,2}, Qi Zhang ^{1,2}, Jia-Run Tu ^{1,2} and Teng-Fei Ge ⁴

¹ Tianjin Center, China Geological Survey, Tianjin 300170, China; lguangyao@mail.cgs.gov.cn (G.-Y.L.); fchao@mail.cgs.gov.cn (C.F.); wjiaying@mail.cgs.gov.cn (J.-Y.W.); zqi@mail.cgs.gov.cn (Q.Z.); tjjarun@mail.cgs.gov.cn (J.-R.T.)

² North China Center for Geoscience Innovation, China Geological Survey, Tianjin 300170, China

³ State Key Laboratory of Geological Processes and Mineral Resources, School of Earth Sciences and Resources, China University of Geosciences, Beijing 100083, China; leigao@cugb.edu.cn

⁴ China Aero Geophysical Survey and Remote Sensing Center for Natural Resources, Beijing 100083, China; gtengfei@mail.cgs.gov.cn

* Correspondence: qiu@cugb.edu.cn (L.Q.); lzhidan@mail.cgs.gov.cn (Z.-D.L.)

Abstract: The closing time of the Paleo-Asian Ocean and the tectonic evolution of the northern margin of the North China Craton are still controversial. The geochronology and geochemistry of the Zhaojinggou monzogranite pluton provide new constraints on the late Paleozoic tectonic evolution and the closure time of the Paleo-Asian Ocean in the southern Central Asian Orogenic Belt (CAOB). The monzogranite yielded a zircon U-Pb age of 286.7 ± 1.2 Ma. Due to the characteristics of low-moderate Mg[#] values (25.87–39.21), low Fe₂O₃^T values (1.13–1.72), and A/CNK > 1, we show that the pluton is weak peraluminous, high in potassium calc-alkaline series, and displays the feature of S-type granite. The total REE content is low, the distribution curve is right dipping, and the LREE is enriched; the δ Eu average value is 1.32 (1.11–1.54). The granite presents relatively high (⁸⁷Sr/⁸⁶Sr)_i values of 0.712345–0.713723, low $\epsilon_{Nd}(t)$ values of –8.89––8.21 (an average value of –8.56), and a T_{DM2} of 1718–1773 Ma. Furthermore, the zircon in situ Hf isotopic analysis shows ¹⁷⁶Hf/¹⁷⁷Hf ratios of 0.282342 to 0.282614, low $\epsilon_{Hf}(t)$ values of –9.27–0.38 (mean –4.74), and a T_{DM2} of 1275–1887 Ma. Additionally, high field strength elements such as Nb, Ta, and Ti are depleted, and large ion lithophile elements, e.g., Rb, Ba, K, and Sr, are enriched. The above features of the Zhaojinggou monzogranite indicate that the pluton was derived from late Paleoproterozoic to Mesoproterozoic lower crustal mafic materials. By discussing the genesis and tectonic implications of the pluton massif, we propose that the Zhaojinggou monzogranite represents a magmatic event caused by the crustal–mantle interaction during the southward subduction of the eastern Paleo-Asian Ocean in the northern margin of the North China Craton during the Early Permian.

Keywords: S-type granite; late Paleozoic; Paleo-Asian Ocean; Zhaojinggou monzogranite pluton; Central Asian Orogenic Belt



Citation: Li, G.-Y.; Qiu, L.; Li, Z.-D.; Gao, L.; Fu, C.; Wang, J.-Y.; Zhang, Q.; Tu, J.-R.; Ge, T.-F. Closure of the Eastern Paleo-Asian Ocean: Constraints from the Age and Geochemistry of Early Permian Zhaojinggou Pluton in Inner Mongolia (North China). *Minerals* **2022**, *12*, 738. <https://doi.org/10.3390/min12060738>

Academic Editors: Sergei Khromykh and Andrei Tsygankov

Received: 19 April 2022

Accepted: 3 June 2022

Published: 9 June 2022

Publisher's Note: MDPI stays neutral with regard to jurisdictional claims in published maps and institutional affiliations.



Copyright: © 2022 by the authors. Licensee MDPI, Basel, Switzerland. This article is an open access article distributed under the terms and conditions of the Creative Commons Attribution (CC BY) license (<https://creativecommons.org/licenses/by/4.0/>).

1. Introduction

The closure time of the eastern Paleo-Asian Ocean in the northern margin of the North China Craton (NCC) is still controversial [1]. A paleomagnetic study showed that the Paleo-Asian Ocean closed before the Early Permian [2]. However, some authors have indicated that the ocean finally closed in the Late Permian to early Middle Triassic [3], and others propose that the final closure time lasted until the middle Late Triassic [4]. Most scholars believe that the Suolun ophiolite belt was the suture zone of the collision between the North China plate (NCC) and the Siberia plate, and its formation was closely

related to the closure of the Paleo-Asian Ocean [1,5–8]. The discovery of Zhaojinggou weak peraluminous S-type granite in the south of the Suolun suture zone is evidence of the existence of syn-collisional granite in the study area (Figure 1a,b), which may provide an opportunity to reconstruct the orogenic process, crustal evolution, and tectonic history of the eastern Paleo-Asian Ocean.

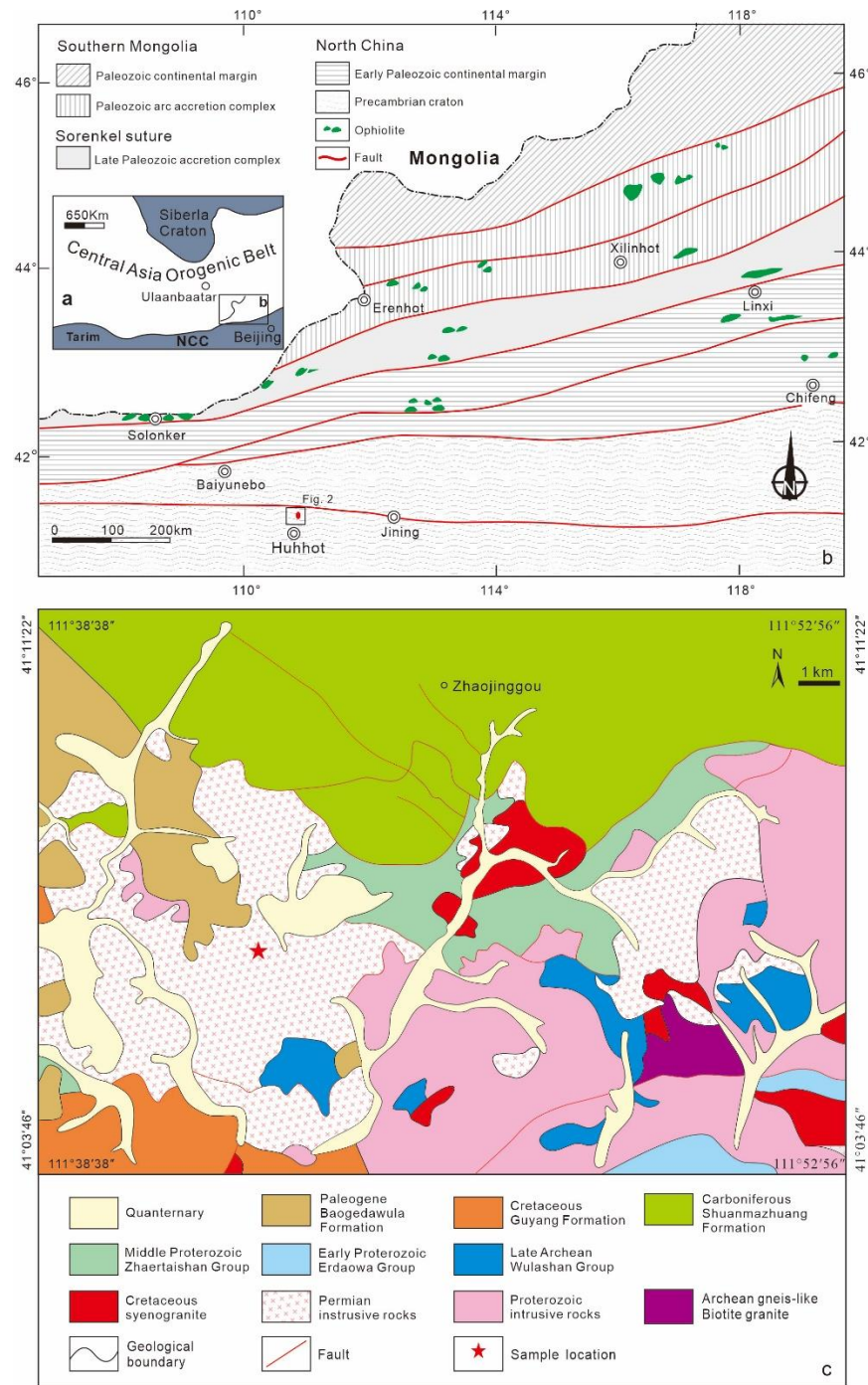


Figure 1. (a) Inset showing the location of the Central Asian Orogenic Belt and adjacent continents; (b) tectonic sketch showing the suture zone and the study area in Inner Mongolia (modified from [1]); (c) geological map of Zhaojinggou pluton and adjacent area (modified from [9]).

In this study, we present the petrology, geochemistry, zircon U-Pb-Hf isotope, and whole-rock Sr-Nd isotopic data to determine the crystallization age, petrogenesis, and

tectonic setting for the Zhaojinggou pluton. The results provide constraints on the timing of the closure of the eastern Paleo-Asian Ocean.

2. Geological Setting

2.1. The Paleo-Asian Ocean and The Central Asian Orogenic Belt (CAOB)

The Paleo-Asian Ocean, located between the Siberia plate and the Tarim-Alashan-North China plate, originated from the cracking of the Neoproterozoic Rodinia supercontinent. Accompanying the reduction and closure of the Paleo-Asian Ocean, the Tarim-Alashan-North China plate and Siberian plate collided and joined together, forming the Central Asian Orogenic Belt [1–3]. The CAOB, which is the Paleo-Asia Ocean tectonic domain, is the largest accretionary orogenic belt in the world [1]. From the Paleozoic to early Mesozoic, this orogenic belt experienced a complex tectonic evolution during the closure of the Paleo-Asian Ocean. It has long been an important window for studying the evolution history of the NCC and the Siberian plate, and it has received extensive attention (e.g., [6–9]).

The northern margin of the NCC is part of the CAOB [10–14]. A large-scale late Paleozoic to early Mesozoic magmatic massif developed in the northern margin of the NCC, sandwiched between the Siberian plate and the NCC. The magmatic massif was a significant record for the subduction and closure of the Paleo-Asian Ocean.

2.2. Regional Geology

The Zhaojinggou pluton is located in the eastern part of Wulashan-Daqingshan in the middle part of the northern NCC and the southern Linhe–Jining fault zone (Figure 1b). The geological evolution events in the area mainly included the Precambrian basement formation, the Mesoproterozoic rifting, the Late Paleozoic–early Mesozoic active continental margin evolution, and the Meso-Cenozoic rifting and uplifting process [15]. The early Precambrian strata are widely developed (Figure 1c; [9]). The late Archean Wulashan Group and the early Proterozoic Erdaowa Group constitute the crystalline basement. The Wulashan Group is mainly composed of amphibolite, amphibolite plagioclase gneiss, magnetite quartzite, granulite, and marble. The Erdaowa Group is a set of metamorphic basic volcanic–sedimentary rocks. The Zhaertaishan Group with low greenschist facies metamorphism formed in the middle Proterozoic rifting environment is widely distributed in the region, and its lithology is phyllite, slate, metamorphic sandstone, and marble. The Upper Carboniferous Shuanmazhuang Formation is widely distributed to the north and is composed of metaconglomerate and variegated metasandstone [16]. The Cretaceous Guyang Formation is exposed locally. The rock association is composed of yellow green conglomerate intercalated with gravelly lithic arkose, medium-grained arkose, coarse-grained lithic sandstone, siltstone, and black carbonaceous shale intercalated with seam.

Paleoproterozoic magmatism was extensive in the region. The Paleoproterozoic granitoid massif is composed of quartz diorite-diorite-hornblende monzonite and developed in the south of the Guyang–Wuchuan fault, Daqingshan Mountain, Inner Mongolia, and the western North China Craton yielded a zircon U-Pb age of 2416–2435 Ma [17]. Phanerozoic granites included Paleozoic biotite granite and granodiorite, such as Xiaojinggou biotite monzogranite that yielded a U-Pb aged 275 ± 1 Ma [18]. Mesozoic syenogranite, porphyry granite, and alkali feldspar granite complex were also mapped in the study area.

2.3. The Zhaojinggou Pluton

The Zhaojinggou pluton is located 2 km east of Wuchuan County, Hohhot city. The exposed area of the Zhaojinggou pluton is about 30 km², and the pluton mainly consists of monzogranite, without obvious lithofacies zoning. The medium-fine grained monzogranite is composed of quartz (25%), plagioclase (35%), potassium feldspar (35%), and scaly biotite (5%). The quartz, plagioclase, and K-feldspar show a xenomorphic granular texture, subhedral albite twins, and euhedral-subhedral plates, respectively.

3. Analytical Methods

3.1. Zircon U-Pb and Hf Isotopes

A representative sample (17ZG-1; 41°06′49.50″ N, 111°42′47.37″ E; Figure 1c) of Zhaojinggou monzogranite was collected for zircon U-Pb dating. The mineral separation was undertaken by Langfang Chengxin Geological Service Co., Ltd. The mounting and CL images of samples were completed in the laboratory of the Tianjin Center, China Geological Survey.

The fresh rock samples were mechanically crushed to 80 mesh, washed with water, magnetically separated, and then washed with alcohol. The single zircon mineral was selected manually; the zircon grains to be tested were made into targets with epoxy resin, and then ground to half of the zircon particles and polished. Zircon U-Pb age and Hf isotope analyses were performed in the Isotope Laboratory of the Tianjin Center, China Geological Survey, using a Neptune (LA-MC-ICPMS) manufactured by Thermo Fisher Scientific, Waltham, MA, USA. The spot diameter was 50 μm . The denudation time was 30 s. Zircon GJ-1 was used as the external standard to calculate the Hf isotope ratios, with a weighted mean $^{176}\text{Hf}/^{177}\text{Hf}$ ratio of 0.282012 ± 35 (2σ , $n = 52$) during our routine analyses. The detailed analytical and calculating procedure followed that of [19,20].

3.2. Whole-Rock Geochemistry

Six fresh rock samples without alteration were collected in the field (17ZG-2-1, 17ZG-2-2, 17ZG-2-3, 17ZG-2-4, 17ZG-2-5, and 17ZG-2-6). Whole-rock major oxides were measured using a PW4400/40 X-ray fluorescence spectrometer (XRF) at the laboratory of the Tianjin Center, China Geological Survey. The detailed analytical procedure is available in [21].

3.3. Rb-Sr and Sm-Nd Isotopic Compositions

Whole rock sample powders of about 200 mesh were dissolved by HF + HClO₄ + HNO₃ and reacted in a closed Teflon sample dissolver at a high temperature for 7 days. Total rare earth was obtained by separating the Rb and Sr from the dissolved sample with AG50W \times 12 strong acid cation exchange resin, and then Sm and Nd elements were separated by HEHEHP resin (P507). The blank background of the whole process was stable at Sm = 3.0×10^{-11} g; Nd = 5.4×10^{-11} g. An Nd isotope ratio test was completed in Triton. The NIST SRM 987 Sr standard and the Jndi-1 Nd standard analyzed together with the international standard rock sample BCR-2 yielded $^{87}\text{Sr}/^{86}\text{Sr} = 0.705019 \pm 0.000005$ (2SE) and $^{143}\text{Nd}/^{144}\text{Nd} = 0.512636 \pm 0.000003$ (2SE), respectively. The detailed analytical procedure is available in [22–24].

4. Analytical Results

4.1. Zircon U-Pb Age

The zircon U-Pb results are shown in Table 1.

The zircon was columnar or ellipsoidal, colorless, and transparent, about 100 μm long and 50 μm wide. The cathodoluminescence image showed oscillatory zoning, and the Th/U ratios were greater than 0.1 (0.58–2.31), indicating magmatic origin. The $^{206}\text{Pb}/^{238}\text{U}$ age ranged from 283 to 292 Ma, and the weighted average age was 286.7 ± 1.2 Ma ($n = 23$; MSWD = 0.87) (Figure 2), representing the crystallization age of Early Permian Zhaojinggou monzogranite.

Table 1. Zircon U-Pb dating data from the Zhaojinggou monzogranite, Inner Mongolia.

Sample Number	Content ($\times 10^{-6}$)		Th/U	Isotope Ratio						Age (Ma)						
	Pb	U		$^{206}\text{Pb}/^{238}\text{U}$	1σ	$^{207}\text{Pb}/^{235}\text{U}$	1σ	$^{207}\text{Pb}/^{206}\text{Pb}$	1σ	$^{206}\text{Pb}/^{238}\text{U}$	1σ	$^{207}\text{Pb}/^{235}\text{U}$	1σ	$^{207}\text{Pb}/^{206}\text{Pb}$	1σ	
Sam.1	26	506	539	1.0658	0.0449	0.0005	0.3282	0.0049	0.0530	0.0007	283	3	288	4	329	29
Sam.2	20	411	240	0.5837	0.0457	0.0005	0.3301	0.0054	0.0524	0.0008	288	3	290	5	305	33
Sam.3	14	257	276	1.0771	0.0457	0.0005	0.3305	0.0062	0.0525	0.0009	288	3	290	5	307	41
Sam.4	29	502	1162	2.314 4	0.0463	0.0005	0.3288	0.0075	0.0515	0.0012	292	3	289	7	264	51
Sam.5	31	620	482	0.7781	0.0458	0.0005	0.3336	0.0053	0.0529	0.0007	288	3	292	5	323	31
Sam.6	26	515	527	1.0216	0.0455	0.0005	0.3307	0.0079	0.0527	0.0013	287	3	290	7	315	57
Sam.7	16	318	345	1.0847	0.0451	0.0005	0.3306	0.0059	0.0531	0.0009	285	3	290	5	335	36
Sam.8	24	465	517	1.1114	0.0459	0.0005	0.3316	0.0055	0.0524	0.0008	289	3	291	5	301	33
Sam.9	35	711	646	0.9091	0.0449	0.0005	0.3292	0.0046	0.0532	0.0006	283	3	289	4	338	28
Sam.10	12	251	180	0.7171	0.0455	0.0005	0.3306	0.0069	0.0527	0.0010	287	3	290	6	317	43
Sam.11	22	370	531	1.4368	0.0463	0.0005	0.3295	0.0071	0.0517	0.0009	292	3	289	6	271	42
Sam.12	24	476	421	0.8845	0.0451	0.0006	0.3339	0.0077	0.0537	0.0010	285	3	293	7	357	42
Sam.13	16	300	378	1.2604	0.0451	0.0005	0.3310	0.0060	0.0532	0.0009	285	3	290	5	337	36
Sam.14	73	1163	2323	1.9973	0.0456	0.0005	0.3307	0.0044	0.0526	0.0006	287	3	290	4	313	27
Sam.15	14	254	310	1.2183	0.0458	0.0005	0.3310	0.0077	0.0525	0.0011	288	3	290	7	306	48
Sam.16	11	229	165	0.7212	0.0453	0.0005	0.3326	0.0076	0.0532	0.0011	286	3	292	7	337	48
Sam.17	11	200	221	1.1072	0.0460	0.0005	0.3308	0.0070	0.0522	0.0010	290	3	290	6	293	45
Sam.18	20	348	452	1.3011	0.0464	0.0005	0.3306	0.0057	0.0517	0.0007	292	3	290	5	272	33
Sam.19	21	426	342	0.8014	0.0449	0.0005	0.3251	0.0055	0.0525	0.0008	283	3	286	5	305	35
Sam.20	15	294	257	0.8739	0.0450	0.0005	0.3270	0.0074	0.0527	0.0011	284	3	287	6	317	48
Sam.21	12	220	219	0.9940	0.0451	0.0005	0.3303	0.0062	0.0532	0.0009	284	3	290	5	336	39
Sam.22	13	257	180	0.6987	0.0455	0.0005	0.3302	0.0064	0.0527	0.0009	287	3	290	6	315	41
Sam.23	12	246	208	0.8456	0.0450	0.0005	0.3304	0.0072	0.0532	0.0011	284	3	290	6	337	45

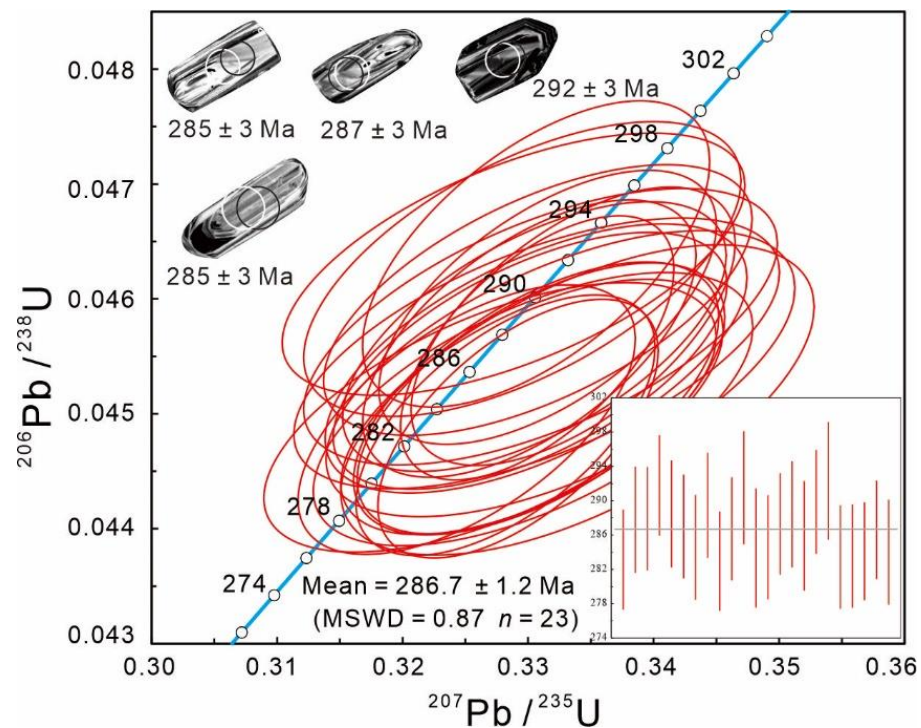


Figure 2. Zircon U-Pb concordia diagram for the sample from the Zhaojinggou monzogranite, Inner Mongolia.

4.2. Whole-Rock Geochemistry

The major and trace elemental compositions of six monzogranite samples from the Zhaojinggou pluton are listed in Table 2.

The samples were all in the granite area (Figure 3a).

Table 2. Major (wt. %) and trace element (ppm) data from the Zhaojinggou monzogranite, Inner Mongolia.

Sample No.	17ZG-2-1	17ZG-2-2	17ZG-2-3	17ZG-2-4	17ZG-2-5	17ZG-2-6	Sample No.	17ZG-2-1	17ZG-2-2	17ZG-2-3	17ZG-2-4	17ZG-2-5	17ZG-2-6
SiO ₂	73.32	75.22	74.44	74.21	72.92	74.60	Sc	0.91	0.84	0.96	1.01	1.42	1.01
Al ₂ O ₃	14.59	13.92	14.09	14.38	14.85	14.08	Nb	6.49	5.75	5.13	6.97	6.06	6.51
Fe ₂ O ₃	1.28	0.70	1.04	1.19	1.12	1.37	Ta	0.57	0.47	0.43	0.58	0.54	0.57
FeO	0.22	0.39	0.42	0.23	0.54	0.30	Zr	92.40	84.90	92.20	89.90	91.20	91.60
CaO	0.59	0.27	0.36	0.36	0.38	0.32	Hf	3.28	2.77	2.92	3.20	3.08	3.13
MgO	0.35	0.21	0.35	0.31	0.56	0.30	Be	1.59	1.47	1.37	1.85	1.46	1.84
K ₂ O	3.51	2.89	3.73	3.35	3.88	3.31	Ga	13.30	12.20	11.80	12.90	15.60	12.50
Na ₂ O	4.40	5.09	4.25	4.46	4.24	4.29	Ge	0.62	0.54	0.63	0.56	0.80	0.77
TiO ₂	0.22	0.21	0.21	0.21	0.21	0.21	U	1.52	0.96	0.64	0.65	0.52	0.70
P ₂ O ₅	0.07	0.06	0.06	0.06	0.07	0.06	Th	7.90	3.92	5.02	6.64	6.26	6.40
MnO	0.05	0.05	0.03	0.05	0.03	0.03	F	294.00	232.00	317.00	292.00	366.00	315.00
LOI	1.39	0.94	0.96	1.16	1.14	1.11	La	18.30	12.80	13.50	10.90	17.20	17.90
Total	99.99	99.96	99.95	99.97	99.94	99.98	Ce	28.60	16.30	27.80	27.50	28.40	29.30
Fe ₂ O ₃ ^T	1.52	1.13	1.51	1.45	1.72	1.70	Pr	3.32	2.46	2.39	1.98	3.18	3.11
FeO ^T	1.37	1.02	1.36	1.30	1.55	1.53	Nd	11.20	8.34	7.97	6.72	10.60	10.40
Mg [#]	31.26	26.85	31.51	29.82	39.21	25.87	Sm	1.68	1.27	1.14	1.01	1.64	1.57
Na ₂ O/K ₂ O	1.25	1.76	1.14	1.33	1.09	1.30	Eu	0.64	0.49	0.55	0.46	0.66	0.52
A/CNK	1.20	1.16	1.20	1.24	1.25	1.25	Gd	1.45	1.06	1.04	0.98	1.42	1.30
A/NK	1.32	1.21	1.28	1.31	1.33	1.32	Tb	0.19	0.14	0.12	0.13	0.18	0.16
Cu	3.28	7.60	6.55	7.43	2.94	6.60	Dy	0.88	0.62	0.58	0.59	0.92	0.70
Pb	14.80	29.60	9.13	6.74	7.95	6.26	Ho	0.16	0.11	0.10	0.11	0.18	0.13
Zn	24.60	13.20	23.40	17.70	30.60	18.60	Er	0.48	0.28	0.28	0.32	0.47	0.35
Cr	7.21	6.97	7.34	5.85	7.10	6.25	Tm	0.07	0.04	0.04	0.05	0.07	0.06
Ni	3.51	7.29	7.18	6.64	5.26	6.79	Yb	0.50	0.27	0.31	0.37	0.52	0.37
Co	2.42	2.14	2.23	2.39	2.48	2.83	Lu	0.08	0.05	0.05	0.06	0.08	0.06
Li	2.46	7.51	2.90	5.18	7.62	6.68	Y	4.49	2.54	2.58	2.69	4.25	3.47
Rb	86.80	54.90	90.00	81.20	101.00	80.00	∑REE	72.04	46.77	58.45	53.87	69.77	69.40
Cs	2.32	2.13	4.67	2.81	6.56	2.01	δEu	5.83	4.34	4.07	3.72	5.71	5.34
Sr	238.00	137.00	290.00	201.00	259.00	186.00	(La/Yb) _N	24.08	31.39	28.79	19.33	21.77	31.81
Ba	1070.00	905.00	1040.00	903.00	1100.00	830.00	(La/Sm) _N	6.63	6.14	7.20	6.56	6.38	6.94
V	17.50	15.90	14.40	19.00	19.80	15.70	(Gd/Yb) _N	2.32	3.16	2.69	2.11	2.19	2.81

Note: All analyzed at Tianjin Institute of Geology and Mineral Resources, Tianjin, China. Mg[#] = 100* Mg²⁺/(Mg²⁺+FeO^T); FeO^T = FeO + 0.8998* Fe₂O₃; ACNK = Al₂O₃/(CaO + Na₂O + K₂O); δEu = Eu_N/(Sm_N × Gd_N)^{1/2}; N = chondrite-normalized; Primitive mantle values are available in [25].

The contents of SiO₂ were high, ranging from 72.92 to 75.22%, the Al₂O₃ contents ranged from 13.92 to 14.85%, and the contents of Na₂O were 4.24 to 5.09%. The contents of CaO were low, ranging from 0.27 to 0.59%, the K₂O values ranged from 2.89 to 3.88%, with an average of 3.45%; the contents of MgO were between 0.21 and 0.56%, with low–moderate Mg[#] values (25.87–39.21) and low Fe₂O₃^T values (1.13–1.72); and the Na₂O/K₂O ratio was 1.09–1.76, with an average of 1.31. The SiO₂–K₂O diagram (Figure 3b) shows calc–alkaline and high-k calc alkaline characteristics. The A/CNK–A/NK diagram (A/CNK: 1.16 to 1.25) shows that the samples were weak peraluminous (Figure 3c).

The trace element spider diagram shows that large ion lithophile elements such as Rb, Ba, K, and Sr were enriched, while high field strength elements such as Nb, Ta, and Ti were depleted (Figure 4a), showing the geochemical properties of subduction zone rocks. The REE distribution curve of granodiorite is obviously right dipping (Figure 4b), the ∑REE value ranged from 46.77 to 72.04 ppm, the (La/Yb)_N value was 19.33–31.81, the LREE was enriched, and the δEu mean value was 1.32 (1.11–1.54), showing a weak Eu positive anomaly.

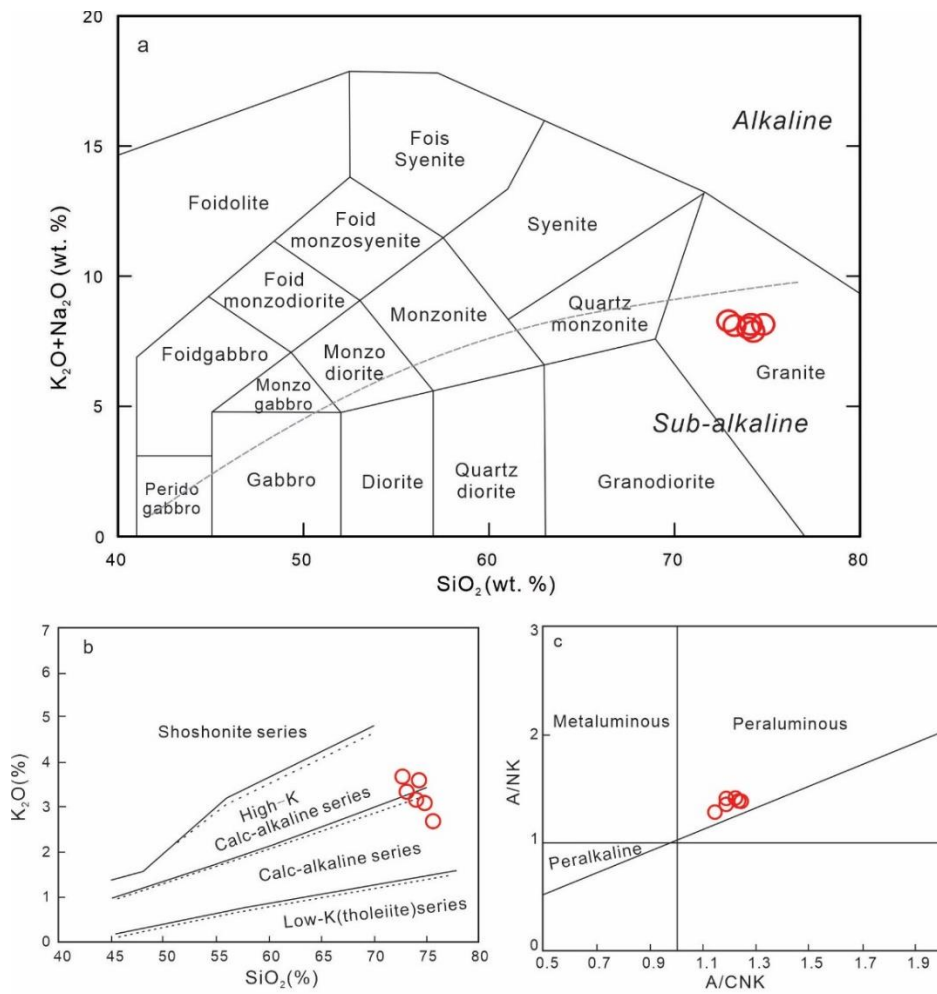


Figure 3. Classification of the samples from Zhaojinggou monzogranite pluton, Inner Mongolia. (a) TAS diagram [26]; (b) SiO₂-K₂O diagram of Zhaojinggou monzogranite, Inner Mongolia [26]; (c) A/CNK-A/NK diagram [27].

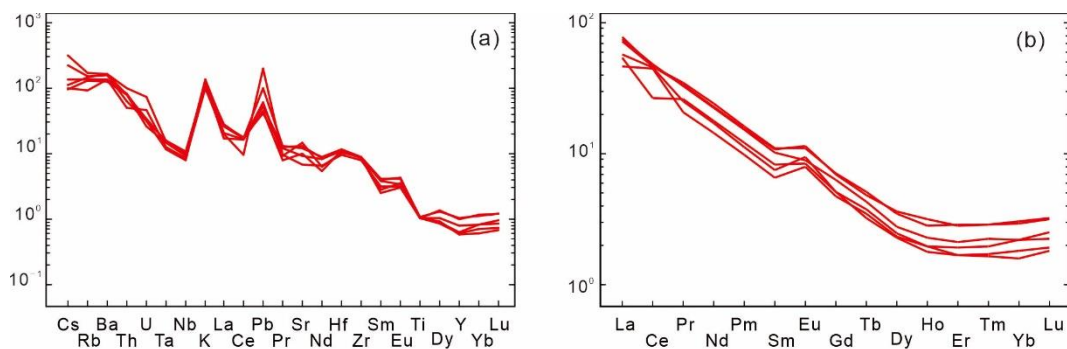


Figure 4. REE and trace elemental diagram of Zhaojinggou monzogranite in Inner Mongolia. (a) Primitive mantle-normalized trace elements spider diagram of Zhaojinggou monzogranites, Inner Mongolia. The values of normalization are from [28]. (b) Chondrite-normalized REE patterns diagram of Zhaojinggou monzogranite, Inner Mongolia (from [25]).

4.3. Zircon Hf Isotopes

Zircon in situ Hf isotopes compositions of monzogranite samples are listed in Table 3.

Table 3. Hf isotopic compositions for zircons of the Zhaojinggou monzogranite, Inner Mongolia.

Spots	t(Ma)	¹⁷⁶ Yb/ ¹⁷⁷ Hf	2σ	¹⁷⁶ Lu/ ¹⁷⁷ Hf	2σ	¹⁷⁶ Hf/ ¹⁷⁷ Hf	2σ	ε _{Hf} (0)	ε _{Hf} (t)	2σ	T _{DM1} (Ma)	T _{DM2} (Ma)	f _{Lu/Hf}
1	283	0.061092	0.000936	0.002117	0.000007	0.282362	0.000027	-14.51	-8.69	0.96	1295	1846	-0.94
2	288	0.032120	0.000213	0.001221	0.000011	0.282425	0.000023	-12.26	-6.18	0.84	1175	1692	-0.96
3	288	0.051916	0.000446	0.001756	0.000011	0.282467	0.000033	-10.79	-4.80	1.16	1133	1605	-0.95
4	292	0.030021	0.000349	0.001061	0.000009	0.282479	0.000024	-10.36	-4.15	0.87	1095	1567	-0.97
5	288	0.024232	0.000140	0.000831	0.000005	0.282473	0.000028	-10.57	-4.39	1.00	1096	1580	-0.97
6	287	0.075826	0.000652	0.002560	0.000012	0.282482	0.000024	-10.25	-4.43	0.87	1135	1581	-0.92
7	285	0.054636	0.001581	0.001844	0.000033	0.282558	0.000026	-7.57	-1.66	0.94	1005	1405	-0.94
8	289	0.047210	0.001065	0.001512	0.000026	0.282567	0.000027	-7.23	-1.16	0.95	982	1377	-0.95
9	283	0.045350	0.000294	0.001772	0.000014	0.282370	0.000024	-14.20	-8.32	0.85	1271	1823	-0.95
10	287	0.034523	0.000199	0.001163	0.000007	0.282507	0.000026	-9.39	-3.31	0.92	1059	1510	-0.96
11	292	0.057211	0.000951	0.001874	0.000024	0.282470	0.000025	-10.70	-4.65	0.89	1132	1598	-0.94
12	285	0.041712	0.001649	0.001415	0.000024	0.282614	0.000026	-5.60	0.38	0.93	914	1275	-0.96
13	285	0.050456	0.000167	0.001582	0.000008	0.282360	0.000024	-14.58	-8.63	0.85	1280	1844	-0.95
14	287	0.052879	0.000320	0.001763	0.000009	0.282528	0.000024	-8.64	-2.66	0.87	1046	1470	-0.95
15	288	0.052959	0.000521	0.002057	0.000027	0.282342	0.000030	-15.21	-9.27	1.06	1322	1887	-0.94
16	286	0.032289	0.000677	0.001211	0.000015	0.282377	0.000023	-13.95	-7.90	0.83	1242	1799	-0.96

Note: $\epsilon_{Hf}(0) = [(^{176}Hf/^{177}Hf)_s / (^{176}Hf/^{177}Hf)_{CHUR,0} - 1] \times 10,000$; $\epsilon_{Hf}(t) = \{ [(^{176}Hf/^{177}Hf)_s - (^{176}Lu/^{177}Hf)_s \times (e^{\lambda t} - 1)] / [(^{176}Hf/^{177}Hf)_{CHUR,0} - (^{176}Lu/^{177}Hf)_s \times (e^{\lambda t} - 1)] - 1 \} \times 10,000$; $T_{DM1} = 1/\lambda \times \ln\{1 + [(^{176}Hf/^{177}Hf)_s - (^{176}Hf/^{177}Hf)_{DM}] / [(^{176}Lu/^{177}Hf)_s - (^{176}Lu/^{177}Hf)_{DM}]\}$; $T_{DM2} = T_{DM1} - (T_{DM1} - t) \times [(f_{cc} - f_s) / (f_{cc} - f_{DM})]$; $f_s = (^{176}Lu/^{177}Hf)_s / (^{176}Lu/^{177}Hf)_{CHUR} - 1$, $(^{176}Lu/^{177}Hf)_s$ and $(^{176}Hf/^{177}Hf)_s$ are the measured value of the samples, $(^{176}Lu/^{177}Hf)_{CHUR} = 0.0332$, $(^{176}Hf/^{177}Hf)_{CHUR,0} = 0.282772$; $(^{176}Lu/^{177}Hf)_{DM} = 0.0384$, $(^{176}Hf/^{177}Hf)_{DM} = 0.28325$, f_{cc} , f_s , f_{DM} represent the average $f_{Lu/Hf}$ from continental crust, samples and depleted mantle, $f_{cc} = -0.55$, $f_{DM} = 0.16$, $\lambda = 1.867 \times 10^{-11} a^{-1}$, $t =$ Formation time of sample zircon.

The zircon in situ Hf isotopic results showed that the ¹⁷⁶Hf/¹⁷⁷Hf ratios ranged from 0.282342 to 0.282614, and the ¹⁷⁶Lu/¹⁷⁷Hf ratios ranged from 0.000831 to 0.002560 (Figure 5a,b). Zircon grains from the monzogranite samples yielded ε_{Hf}(t) values of -9.27–0.38 (mean -4.74), a T_{DM1} of 914–982 Ma, and a T_{DM2} of 1275–1887 Ma.

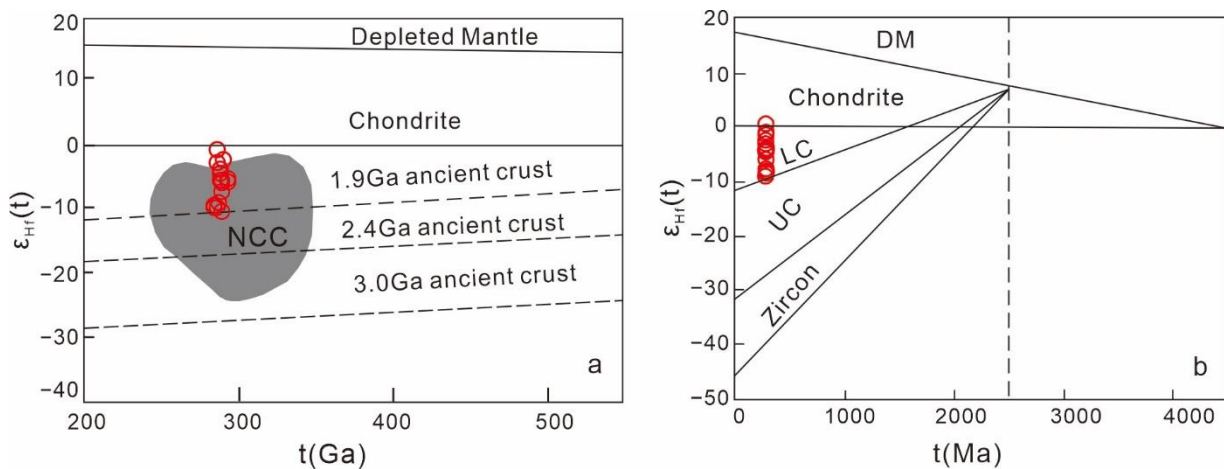


Figure 5. ε_{Hf}(t)-t diagrams of the Zhaojinggou monzogranite. (a) Hf isotope contrast with NCC; the gray field indicates Carboniferous–Permian intrusive rocks on the northern margin of the NCC (after [29]). (b) Hf isotope evolution.

4.4. Whole-Rock Rb-Sr and Sm-Nd Isotopic Compositions

The whole-rock Sr–Nd isotopic compositions for Zhaojinggou monzogranite samples are listed in Table 4 and illustrated in Figure 6.

The initial Sr–Nd isotopic compositions of granites were rectified by the corresponding zircon U–Pb age of 286.7 Ma. The ⁸⁷Sr/⁸⁶Sr values of granites ranged from 0.715233 to 0.716612, and the average value was 0.7160, which was obviously higher than the original mantle value (⁸⁷Sr/⁸⁶Sr = 0.7045, [23]). The ¹⁴³Nd/¹⁴⁴Nd values of granites ranged from 0.511989 to 0.512021, and the average value was 0.512000, which was slightly lower than the original mantle value (¹⁴³Nd/¹⁴⁴Nd = 0.512638, [24]). On the basis of the zircon U–Pb ages, the granite samples had (⁸⁷Sr/⁸⁶Sr)_i values of 0.712345–0.713723, an average value

of 0.7128; $\epsilon_{\text{Nd}}(t)$ values of -8.89 – -8.21 , an average value of -8.56 ; and the T_{DM2} was 1718–1773 Ma.

Table 4. Whole-rock Sr-Nd isotopic composition of the Zhaojinggou monzogranite, Inner Mongolia.

Sampe No.	Rock	Age(Ma)	$^{87}\text{Rb}/^{86}\text{Sr}$	$^{87}\text{Sr}/^{86}\text{Sr}$	2σ	$(^{87}\text{Sr}/^{86}\text{Sr})_i$	$^{147}\text{Sm}/^{144}\text{Nd}$	$^{143}\text{Nd}/^{144}\text{Nd}$	2σ	$\epsilon_{\text{Nd}}(t)$	$T_{\text{DM}}(\text{Ma})$	$T_{\text{DM2}}(\text{Ma})$
17ZG-2-1	Monzogranite	286.7	0.708098	0.716612	0.000009	0.713723	0.090670	0.511996	0.000007	-8.65	1427.5	1754
17ZG-2-2	Monzogranite	286.7	0.707833	0.715951	0.000007	0.713063	0.092048	0.512021	0.000008	-8.21	1412.5	1718.4
17ZG-2-3	Monzogranite	286.7	0.707661	0.715614	0.000009	0.712727	0.086461	0.512001	0.000010	-8.40	1374.6	1733.8
17ZG-2-4	Monzogranite	286.7	0.708033	0.715233	0.000007	0.712345	0.090850	0.511997	0.000008	-8.63	1428.4	1752.9
17ZG-2-5	Monzogranite	286.7	0.707985	0.715373	0.000008	0.712485	0.093521	0.511989	0.000003	-8.89	1470.1	1773.4
17ZG-2-6	Monzogranite	286.7	0.708507	0.715373	0.000009	0.712483	0.091251	0.512000	0.000004	-8.59	1429.3	1749.3

Note: $(^{87}\text{Rb}/^{86}\text{Sr})_{\text{CHUR}} = 0.0847$; $(^{87}\text{Sr}/^{86}\text{Sr})_{\text{CHUR}} = 0.7045$; $(^{147}\text{Sm}/^{144}\text{Nd})_{\text{CHUR}} = 0.1967$; $(^{143}\text{Nd}/^{144}\text{Nd})_{\text{CHUR}} = 0.512638$ ([30]); t -Diagenetic age.

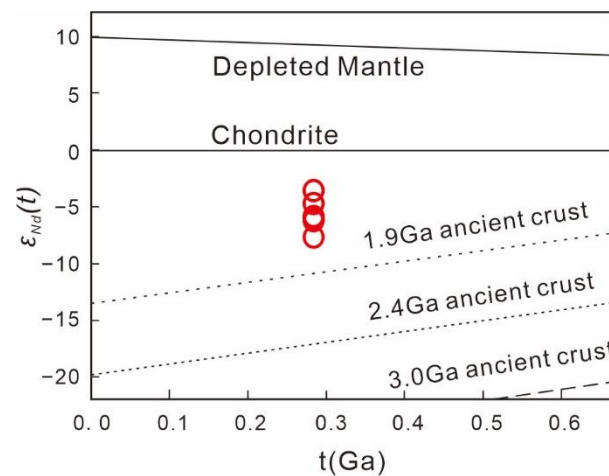


Figure 6. $\epsilon_{\text{Nd}}(t)$ - t diagrams of the Zhaojinggou monzogranite.

5. Discussion

5.1. Timing of the Magmatism on Northern NCC in Early Permian

Magma is the carrier of material and energy exchange in plate activity; its composition, distribution, and evolution have a close relationship with the tectonic environment, and it is often used to reconstruct the paleotectonic environment [31]. The southward subduction of the Paleo-Asian oceanic crust and subsequent collision caused a large number of magmatic records in the northern margin of the NCC [11]. Large-scale magmatic plutons occurred in the Early Permian in the northern NCC, stretching for hundreds of kilometers from west to east, including the Wulatzhongqi biotite monzogranite (279 ± 3 Ma, [15]); the Bayan Obo granodiorite and biotite granite (269 ± 3 Ma, 268 ± 2 Ma, [32]); the Siziwangqi syenogranite and biotite granodiorite (264 ± 3 Ma, 267 ± 9 Ma, [33]); and the granodiorite and diorite in the Chengde area (288 ± 2 Ma, [34]). These ages prove extensive late Permian magmatic events in the northern NCC, indicating strong subduction and signs of oceanic ridge-trench collision [10].

In this study, we obtained the Late Permian crystallization age of the Zhaojinggou monzogranite pluton (286.7 ± 1.2 Ma), which is basically consistent with the above ages from the northern NCC. These magmatic records are an important basis for determining the closing time limit of the Paleo-Asian Ocean.

5.2. Petrogenesis of the Zhaojinggou Granite Pluton

On the AMF-CMF petrogenetic diagram, the samples are distributed in the zone of partial melts of metapelitic sources, near the left boundary of partial melts from meta-greywackes (Figure 7a), indicating that sedimentary rocks rich in aluminum may be the source [35].

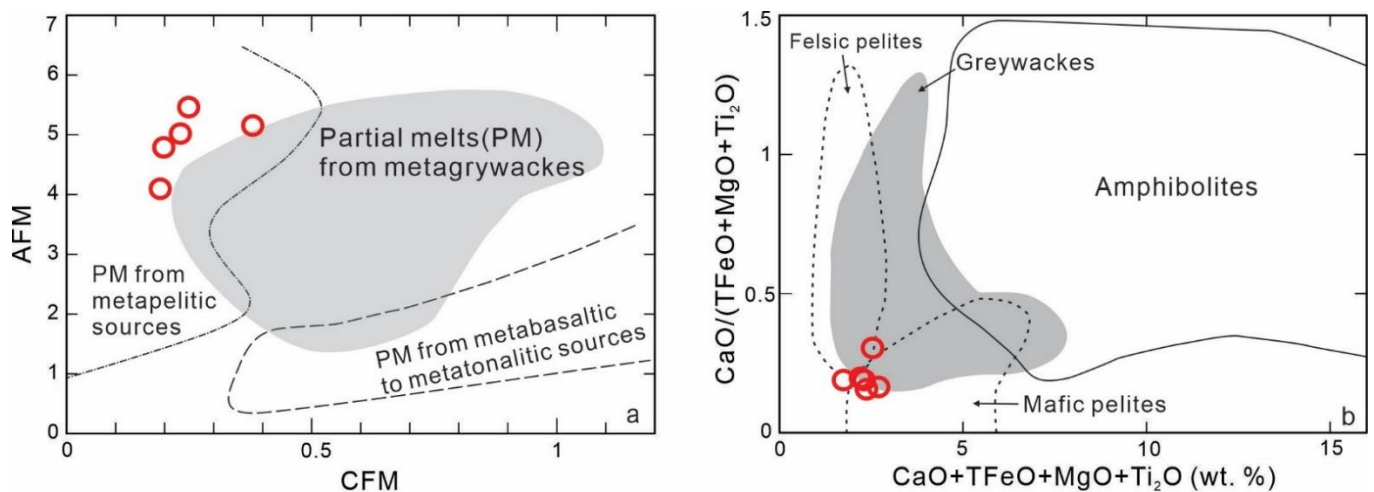


Figure 7. Diagrams for the petrogenesis of the Zhaojinggou monzogranite. (a) AMF (molar $\text{Al}_2\text{O}_3/(\text{MgO} + \text{TFeO})$) versus CMF (molar $\text{CaO}/(\text{MgO} + \text{TFeO})$) diagram (from [25]); (b) $\text{CaO}/(\text{TFeO} + \text{MgO} + \text{TiO}_2)$ versus $\text{CaO} + \text{TFeO} + \text{MgO} + \text{TiO}_2$ diagram (modified from [30]).

Furthermore, all of the samples were plotted within or near the field of mafic pelites or greywackes (Figure 7b), indicating that the source rocks experienced intracrustal recycling [36]. Additionally, the samples with the middling fractionated REE patterns and smooth HREE patterns may have originated from mid-crustal materials containing plagioclase or plagioclase + biotite. The obviously geochemical characteristics of high-K calc-alkaline, $A/\text{CNK} > 1$, enrichment in LREE and LILE, and depletion in HFSE may reveal the features of Andean-type continental arc magmas. Combined with the low Sr isotope content (< 300 ppm) and sedimentary origin, it can be further inferred that the pluton is S-type granite, which is usually produced in a subduction environment [37].

Moreover, the characteristics of the low–moderate $\text{Mg}^\#$ values (25.87–39.21), low Fe_2O_3^T values (1.13–1.72), weak positive δEu average values of 1.32 (1.11–1.54), relatively high $(^{87}\text{Sr}/^{86}\text{Sr})_i$ values of 0.712345–0.713723, low $\epsilon_{\text{Nd}}(t)$ values of -8.89 – -8.21 (average value of -8.56), a $T_{\text{DM}2}$ of 1718–1773 Ma (Figure 6), low $\epsilon_{\text{Hf}}(t)$ values of -9.27 – -0.38 (mean -4.74), a $T_{\text{DM}2}$ of 1275–1887 Ma, and the points of $\epsilon_{\text{Hf}}(t)$ - t primitively falling within the range of the Carboniferous–Permian intrusive rocks on the northern margin of the NCC (Figure 5a) indicate that the pluton was derived from late Paleoproterozoic to Mesoproterozoic lower crustal mafic materials in the NCC.

5.3. Tectonic Implications

The tectonic evolution of the northern margin of the NCC during the Permian period has been a controversial issue [4]. Zhou et al. (2019) [38] hold that the tectonic system of the northern margin of the North China Craton changed from a subduction (pre-275 Ma) to post-collision extension (275–255 Ma). In contrast, the arc–trench system within the ocean played a leading role during the Permian [10]. The origin of the Zhaojinggou granite pluton provides new constraints on the tectonic evolution of the northern margin of NCC in the eastern margin of the Paleo-Asian Ocean. According to the zircon Hf isotopes, negative $\epsilon_{\text{Hf}}(t)$ values, and various $T_{\text{DM}2}(\text{Hf})$ ages (1275–1887 Ma), the metapelite–metagreywacke protolith of the Zhaojinggou pluton could have been formed due to Mesoproterozoic sources with suptasubduction affinity. The geochemical results suggest that the granite had Ni, Nb, and Ti negative abnormality, indicating the involvement of oceanic sediments. Therefore, we propose that the pluton was derived from partial melting of the lower crust in an active continental margin environment during the late Paleoproterozoic southward subduction of the Paleo-Asian Oceanic lithosphere. Additionally, Zhang et al. holds that the gabbroic diorite (291.1 ± 1.8 Ma) located in the Zhaojinggou area was derived from the subduction-related enriched subcontinental lithospheric mantle (SCLM) [39].

Wang et al. (2007) [34] also suggest that the northern margin of the NCC was an Andean active continental margin in the Early Permian by studying the diorite plutons (288 Ma, consistent with the age in this article) that intruded in the late Paleozoic. Furthermore, a classical model [40] can well explain the genesis of the pluton: dehydration of the subduction plate → uneven hydration of the mantle wedge → rising of the mantle-derived magma → crust melting → differentiation and crystallization of magmas (Figure 8a). Here, the Zhaojinggou granite pluton yielded a zircon U-Pb age of ~287 Ma and indicates Early Permian emplacement. Thus, we propose the Paleo-Asian Ocean did not shut until the Early Permian in the northern margin of the NCC (Figure 8b).

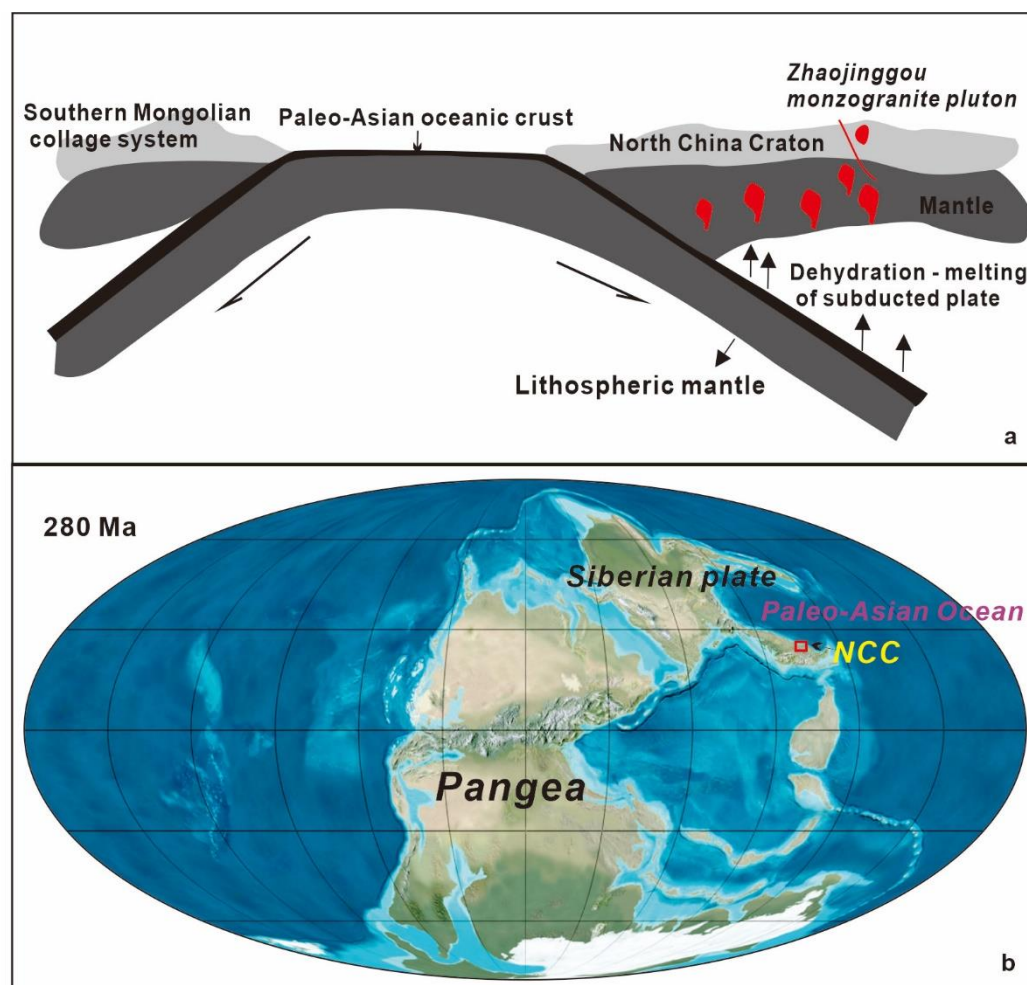


Figure 8. (a) Schematic diagram of the tectonic setting for the Zhaojinggou area in the northern NCC during the Early-Middle Permian (modified from [1,6,40]). (b) The Paleogeographic earth reconstruction, Early Permian (modified from [41]).

6. Conclusions

1. The Zhaojinggou pluton yielded a zircon U-Pb age of 286.7 ± 1.2 Ma, indicating an Early Permian magmatism.
2. The Zhaojinggou monzogranite was derived from lower crustal melting in a continental arc setting, suggesting the closure of the eastern Paleo-Asian Ocean in the north margin of the NCC postdated the Early Permian.

Author Contributions: Conceptualization: G.-Y.L., L.Q. and Z.-D.L.; methodology: L.G. and J.-R.T.; software: Q.Z. and T.-F.G.; validation: L.Q. and J.-Y.W.; investigation: G.-Y.L., Z.-D.L. and C.F.; data curation: G.-Y.L.; writing—original draft preparation: G.-Y.L., L.Q. and Z.-D.L.; writing—review and editing: G.-Y.L. and L.Q. All authors have read and agreed to the published version of the manuscript.

Funding: This research was funded by the China Geological Survey (Grant No.12120113057300; DD20190119; DD20211191; DD20221686) and National Natural Science Founding of China (Grant No.41502082).

Institutional Review Board Statement: Not applicable.

Informed Consent Statement: Not applicable.

Data Availability Statement: Not applicable.

Conflicts of Interest: The authors declare no conflict of interest.

References

1. Xiao, W.J.; Windley, B.F.; Hao, J.; Zhai, M.G. Accretion Leading to Collision and the Permian Solonker Suture, Inner Mongolia, China: Termination of the Central Asian Orogenic Belt. *Tectonics* **2003**, *22*. [[CrossRef](#)]
2. Zhao, P.; Appel, E.; Xu, B.; Sukhbaatar, T. First Paleomagnetic Result from the Early Permian Volcanic Rocks in Northeastern Mongolia: Evolutional Implication for the Paleo-Asian Ocean and the Mongol-Okhotsk Ocean. *J. Geophys. Res. Solid Earth* **2020**, *125*, 1–16. [[CrossRef](#)]
3. Xiao, W.J.; Windley, B.F.; Sun, S.; Li, J.L.; Huang, B.C.; Han, C.M.; Yuan, C.; Sun, M.; Chen, H.L. A Tale of Amalgamation of Three Permo-Triassic Collage Systems in Central Asia: Oroclines, Sutures, and Terminal Accretion. *Annu. Rev. Earth Planet. Sci.* **2015**, *43*, 477–507. [[CrossRef](#)]
4. Shao, J.A.; He, G.Q.; Tang, K.D. The Evolution of Permian Continental Crust in Northern Part of North China. *Acta Petrol. Sin.* **2015**, *31*, 47–55.
5. Li, J.Y. Permian geodynamic setting of Northeast China and adjacent regions: Closure of the Paleo-Asian Ocean and subduction of the Paleo-Pacific Plate. *J. Asian Earth Sci.* **2006**, *26*, 207–224. [[CrossRef](#)]
6. Windley, B.F.; Alexeiev, D.; Xiao, W.J.; Kröner, A.; Badarch, G. Tectonic models for accretion of the Central Asian Orogenic Belt. *J. Geol. Soc.* **2007**, *164*, 31–47. [[CrossRef](#)]
7. Chen, B.; Jahn, B.M.; Tian, W. Evolution of the Solonker suture zone: Constraints from zircon U-Pb ages, Hf isotopic ratios and whole-rock Nd-Sr isotope compositions of subduction- and collision-related magmas and forearc sediments. *J. Asian Earth Sci.* **2009**, *34*, 245–257. [[CrossRef](#)]
8. Xiao, W.J.; Huang, B.C.; Han, C.M.; Sun, S.; Li, J.Y. A review of the western part of the Altaids: A key to understanding the architecture of accretionary orogen. *Gondwana Res.* **2010**, *18*, 253–273. [[CrossRef](#)]
9. Li, Z.D.; Li, X.G.; Cui, Y.R.; Li, G.Z.; Zhang, J.; Guo, H.; Liu, W.G.; Zhang, C.; Yu, R.A.; Xie, Y.; et al. Yanshanian Mineralization of Zhaojinggou Nb-Ta Deposit, Wuchuan County, Inner Mongolia: Evidences from the Monazite and Zircon LA-MC-ICP-MS U-Pb and biotite ⁴⁰Ar-³⁹Ar geochronology. *Earth Sci.* **2019**, *41*, 234–247. [[CrossRef](#)]
10. Jian, P.; Liu, D.Y.; Alfred, K.; Brian, F.; Windley Shi, Y.R.; Zhang, W.; Zhang, F.Q.; Miao, L.C.; Zhang, L.Q.; Dondov, T. Evolution of a Permian Intraoceanic Arc-trench System in the Solonker Suture Zone, Central Asian Orogenic Belt, China and Mongolia. *Lithos* **2010**, *118*, 169–190. [[CrossRef](#)]
11. Wang, S.J.; Xu, Z.Y.; Dong, X.J.; Wang, W.Q. Geochemical Characteristics and Zircon U-Pb Age of the Granodiorite-Norite Gabbro in the Northern Margin of the North China Block North China plate and Their Formation Mechanism. *Earth Sci.* **2018**, *43*, 3267–3284. [[CrossRef](#)]
12. Chu, H.; Zhang, J.R.; Wei, C.J.; Wang, H.C.; Kang, J.L. Multiple Phases of Metamorphism during Paleozoic-Mesozoic and the Implication for the Tectonic Evolution of Northern North China: Research Progresses and Prospects of “The Paleozoic Metamorphism and Tectonic Dynamics in North China”. *Geol. Surv. Res.* **2020**, *43*, 186–197. [[CrossRef](#)]
13. Yuan, G.B.; Wang, H.C. Magmatic Activity and Its Tectonic Implications During the Early Permian in the Northwestward of Wuchuan, Inner Mongolia. *Geol. Surv. Res.* **2006**, *29*, 303–310.
14. Chen, Y.J.; Zhai, M.G.; Jiang, S.Y. Significant Achievements and Open Issues in Study of Orogenesis and Metallogenesis Surrounding the North China Continent. *Acta Petrol. Sin.* **2009**, *25*, 2695–2726. [[CrossRef](#)]
15. Wang, H.C.; Xiang, Z.Q.; Zhao, F.Q.; Li, H.M.; Chu, H. The Alkaline Plutons in Eastern Part of Guyang County, Inner Mongolia: Geochronology, Petrogenesis and Tectonic Implications. *Acta Petrol. Sin.* **2012**, *28*, 284–2854. [[CrossRef](#)]
16. Chai, H.; Li, Z.J.; Zhu, G.F.; Men, B.T.; Su, K.; Su, Y.C. *Exploration Report of Zhaojinggou Nb-Ta Deposit, Wuchuan County, Inner Mongolia*; Inner Mongolia First Geological Mineral Exploration Institute: Hohhot, China, 2013.
17. Zhong, C.T.; Deng, J.F.; Wan, Y.S.; Tu, W.P. Paleoproterozoic Granitoids in the Daqingshan Mountain Area, Inner Mongolia: Geochemistry, SHRIMP Zircon Dating and Geological Significance. *Acta Petrol. Sin.* **2014**, *30*, 3172–3188. [[CrossRef](#)]
18. Mo, N.; Guo, L.; Tong, Y.; Wang, T.; Liu, J.; Li, J.B. Geochronology, Geochemistry, Hf Isotope of Xiaojinggou Pluton in the Northern Margin of North China Craton and Its Tectonic Implications. *Acta Sci. Nat. Univ. Pekin.* **2014**, *50*, 1021–1034. [[CrossRef](#)]

19. Li, H.K.; Geng, J.Z.; Hao, S.; Zhang, Y.Q.; Li, H.M. Determination of zircon U-Pb isotopic age by laser ablation multi-receiver plasma mass spectrometer (LA-MC-ICPMS). *Acta Mineral. Sin.* **2009**, *29*, 600–601.
20. Geng, J.Z.; Li, H.K.; Zhang, J.; Zhou, H.Y.; Li, H.M. Zircon Hf isotope analysis by means of LA-MC-ICP-MS. *Geol. Bull. China* **2011**, *30*, 1508–1513.
21. Gao, J.F.; Lu, J.J.; Lai, M.Y.; Lin, Y.P.; Pu, W. Analysis of trace elements in rock samples using HR-ICPMS. *J. Nanjing Univ. Nat. Sci.* **2003**, *39*, 844–850.
22. Liu, W.G.; Wei, S.; Zhang, J.; Ao, C.; Liu, F.T.; Cai, B.; Zhou, H.Y.; Yang, J.L.; Li, C.F. An improved separation scheme for Sr through fluoride coprecipitation combined with a cation-exchange resin from geological samples with high Rb/Sr ratios for high-precision determination of Sr isotope ratios. *J. Anal. At. Spectrom.* **2020**, *35*, 953–960. [[CrossRef](#)]
23. Depaolo, D.J.; Wasserburg, G.J. Inferences about magma sources and mantle structure from variations of $^{143}\text{Nd}/^{144}\text{Nd}$. *Geophys. Res. Lett.* **1976**, *3*, 743–746. [[CrossRef](#)]
24. Jacobsen, S.B.; Wasserburg, G.J. Sm-Nd isotopic evolution of chondrites and achondrites, II. *Earth Planet. Sci. Lett.* **1984**, *67*, 137–150. [[CrossRef](#)]
25. Sun, S.S.; Macdonough, W.F. Chemical and Isotopic Systematics of Oceanic Basalts: Implications for Mantle Composition of the Earth and Mantle Evolution. *Earth Planet. Sci. Lett.* **1989**, *35*, 429–448. [[CrossRef](#)]
26. Le Maitre, R.W.; Streckeisen, A.; Zanettin, B.; Le Bas, M.J.; Bonin, B.; Bateman, P. *Igneous Rocks: A Classification and Glossary of Terms*; Cambridge University Press: Cambridge, UK, 2010.
27. Maniar, P.D.; Piccoli, P.M. Tectonic discrimination of granitoids. *Geol. Soc. Am. Bull.* **1989**, *101*, 635–643. [[CrossRef](#)]
28. McDonough, W.F.; Sun, S.S. The Composition of the Earth. *Chem. Geol.* **1995**, *120*, 223–253. [[CrossRef](#)]
29. Zhang, S.H.; Zhao, Y.; Liu, J.M.; Hu, Z.C. Different sources involved in generation of continental arc volcanism: The Carboniferous-Permian volcanic rocks in the northern margin of the north China block. *Lithos* **2016**, *240*, 382–401. [[CrossRef](#)]
30. Hart, S.R. A large-scale isotope anomaly in the Southern Hemisphere mantle. *Nature* **1984**, *309*, 753–757. [[CrossRef](#)]
31. Zhang, X.H.; Wilde, S.A.; Zhang, H.F. Early Permian High-K Calc-Alkaline Volcanic Rocks from NW Inner Mongolia, North China: Geochemistry, Origin and Tectonic Implications. *J. Geol. Soc.* **2011**, *168*, 525–543. [[CrossRef](#)]
32. Fan, H.R.; Hu, F.F.; Yang, K.F.; Wang, K.Y.; Liu, Y.S. Geochronology Framework of Late Paleozoic Dioritic-Granitic Plutons in the Bayan Obo Area, Inner Mongolia, and Tectonic Significance. *Acta Petrol. Sin.* **2009**, *25*, 2933–2938.
33. Liu, Y.S.; Gao, S.; Hu, Z.C.; Gao, C.G.; Zong, K.Q.; Wang, D.B. Continental and Oceanic Crust Recycling-induced Melt-peridotite Interactions in the Trans-North China Orogen: U-Pb Dating, Hf Isotopes and Trace Elements in Zircons from Mantle Xenoliths. *J. Petrol.* **2010**, *51*, 537–571. [[CrossRef](#)]
34. Wang, H.C.; Zhao, F.Q.; Li, H.M.; Sun, L.X.; Miao, L.C.; Ji, S.P. Zircon SHRIMP U-Pb age of the dioritic rocks from northern Hebei: The geological records of late Paleozoic magmatic arc. *Acta Petrol. Sin.* **2007**, *23*, 597–604.
35. Altherr, R.; Holl, A.; Hegner, E. High-potassium, Calc-Alkaline I-Type Plutonism in the European Variscides: Northern Vosges (France) and Northern Schwarzwald (Germany). *Lithos* **2000**, *50*, 51–73. [[CrossRef](#)]
36. Patiño-Douce, A.E. What Do Experiments Tell Us about the Relative Contributions of Crust and Mantle to the Origin of Granitic Magmas? *Geol. Soc. Lond. Spec. Publ.* **1999**, *168*, 55–75. [[CrossRef](#)]
37. Zhai, M.G. Granites: Leading study issue for continental evolution. *Acta Petrol. Sin.* **2017**, *33*, 1369–1380.
38. Zhou, H.; Zhao, G.C.; Li, J.H.; Han, Y.G.; Yao, J.L.; Wang, B. Magmatic Evidence for Middle-late Permian Tectonic Evolution on the Northern Margin of the North China Craton. *Lithos* **2019**, *336*, 125–142. [[CrossRef](#)]
39. Zhang, L.; Jiang, S.Y. Early Permian continental arc magmatism in the Zhaojingou area of the northern North China Craton: Implications for crust-mantle interactions during southward Paleo-Asian plate subduction. *Lithos* **2021**, *390*, 106110. [[CrossRef](#)]
40. Hildreth, W.; Moorbath, S. Crustal contributions to arc magmatism in the Andes of Central Chile. *Contrib. Mineral. Petrol.* **1988**, *98*, 455–489. [[CrossRef](#)]
41. SIA3669: Paleogeographic Earth Reconstruction, Early Permian (280 Ma). Available online: <https://scienceviews.com/photo/library/SIA3669.html> (accessed on 27 May 2010).